Electronic Journal of Structural Engineering

Original Article

Cite this: DOI:10.56748/ejse.26819

Received Date: 3 May 2025
Accepted Date: 25 December 2025

1443-9255
https://ejsei.com/ejse

Assessment of Seismic Behavior of Steel Moment Frames Equipped with S-Shaped Steel Plate Dampers

Chunhong YANG [a*] Hongjun ZHUANG [a] Hang DU [a]

[a] School of Mechanical Engineering, Changchun Guanghua University, Changchun 130033, China
*Corresponding author: yanghong19821118@163.com

Abstract

One of the applications of yielding dampers is to boost the productivity of steel structures. Moment-Resisting Frames (MRF) located in areas with high seismicity need to be retrofitted in many cases, and by using this method, the objectives required to achieve seismic performance can be provided at a low cost. The performance of the SSPD as a new bending damper type for retrofitting steel dual-plate MRFs is examined herein. For this purpose, three structures with different heights have been selected. Utilizing the outcomes of linear static analysis with the force tactic, dampers with appropriate dimensions have been designed for the story of these structures. The curves of these dampers have been extracted using nonlinear finite element models in cyclic loading, performed using Analysis by Automatic Quadratic Solver (ABAQUS), and their behavior, including deformation, initial stiffness, and maximum force, has been determined. Then, the extracted nonlinear models were used in the nonlinear models of structures equipped with this type of damper developed in PERFORM software. Nonlinear time history analyses were conducted on structures with and without dampers, and seismic response parameters, including base shear, maximum displacement, drift, and dissipated energy, were compared. The outcomes reveal that, on average, the maximum displacement is 55% lower in structures with dampers. In addition, the maximum drift is less than 44% on average. Finally, it was found that the S-shaped damper dissipates an average of 79% to 93% of seismic energy, which displays its efficiency..

Keywords

SSPD, Seismic retrofitting, Energy dissipation, Drift reduction, Base shear

1. Introduction

Recent applications of seismic control techniques for reducing and preventing earthquake damage have increased dramatically. These means are classified into different types, and damping passive control (DPC) systems are one of the most effective methods (Curadelli and Amani, 2014; Saaed et al., 2015). Much of the seismic force is dissipated by dampers, protecting other areas of the structure from damage if integrated into a building design. Diverse forms of dampers have been studied for some time, including viscous, viscoelastic, and frictional dampers (De Domenico et al., 2019; Gagnon et al., 2020; Jaisee et al., 2021; Shu et al., 2022; Zhang et al., 2024). Other passive strategies, such as buckling braces, self-centering devices (SCDs), and shape memory alloys, have also been studied in recent years as novel approaches to achieving improved seismic performance (Fang et al., 2023; Haider and Lee, 2021; Ke et al., 2023).

Passive seismic control systems, particularly yielding dampers, encompass a wide variety of devices for which extensive literature exists; several types have been developed. They are usually fabricated from metals or some special ductile alloy materials, which exhibit their desirable energy dissipation capacities on account of the yielding characteristics (Javanmardi et al., 2019; Zhang et al., 2015). Based on their internal actions, yielding dampers are generally classified according to the type of force they generate (Shen et al., 2017). One of the most prominent types is the bending plate damper, with ADAS dampers being a notable example (Khoshkalam et al., 2022; Mohammadi et al., 2017). Another set is composed of axially acting dampers, which are primarily employed in bracing systems to enhance ductility and energy dissipation (Hsu and Halim, 2018; Zhao et al., 2021). Shear-yielding, energy-dissipating dampers are also standard. The shear panel dampers are a classical example of this behavior (Zhu et al., 2018, 2023). Some recent studies have even addressed dampers, which are subjected to the combined action of shear and bending to increase their nonlinearity (Jeong et al., 2024; Pan et al., 2024; Sahoo et al., 2015; Zhao et al., 2022). Another category is formed by dampers of special shapes, such as pipe, box, and piston dampers, which create torsional or bending moments, depending on their specific shape arrangements (Cheraghi and Zahrai, 2019; Ghadami et al., 2024; Ghandil et al., 2022). Among the latest developments in damper technology are the S-shaped dampers, made by cold-rolling flat plates. This design increases deformation capacity and nonlinear behavior, improving the seismic performance of structures (Guo et al., 2025b; Zhai et al., 2022, 2020). In other studies, alternative configurations of S-shaped dampers have been examined, in which U-shaped components are interconnected using bolts. This construction approach enhances both the deformation capacity and the load-bearing resistance of the damper and, when combined with other seismic protection systems—such as base isolation—can provide effective protection for buildings against seismic actions (Guo et al., 2025b, 2025a).

The application of yielding dampers as a retrofitting strategy for various structural systems has been widely investigated and recognized as an efficient and cost-effective approach (Khoshkalam et al., 2022; Rakan-Nasrabadi et al., 2025; Shen et al., 2017; Zhang et al., 2015). Recently, the use of diverse dampers to modify the seismic response in Reinforced Concrete Moment-Resisting Frames (RCMRFs) subjected to various types of excitations has been extensively researched (Bruschi and Quaglini, 2022; Foyouzati, 2024; Zhang et al., 2018).

In steel buildings, where various types of bracings are used depending on the location, the use of a yielding damper in the bracing-core system has been widely investigated. Investigations of steel frames with semi-rigid connections indicate that their seismic behavior is highly dependent on the response of the connections (De'nan et al., 2025; Elhout, 2022; Wang et al., 2024). Therefore, installing yielding dampers on these connections may work effectively to improve both the strength and ductility of the structure.

Another common application involves steel moment-resisting frames, in which dampers are typically incorporated as an additional system using chevron bracing. The energy-dissipation action of these dampers, which are nonlinear due to their mechanical nature, can have a significant impact on the global seismic response of the building (Akbar et al., 2021; Cheraghi et al., 2023; Ebadi Jamkhaneh et al., 2019; Fujii, 2024).

Connecting yielding dampers to a structure as a retrofitting method changes seismic behavior. The connection between the damper and the structure varies for different types of dampers and the actions produced by their forces, resulting in modifications to the seismic characteristics of the structure. Given this, the behavior of retrofitted structures under these conditions should be examined with greater precision to appraise the actual efficacy of the damper. This research investigates the effect of using an SSPD as a ductile structural fuse with acceptable nonlinear behavior in the retrofitting of medium-rise steel MRFs located in areas with high seismicity. To achieve this, several structures with varying numbers of stories were designed, utilizing a moment frame as the lateral bearing system. In the next step, utilizing the seismic requirements of the structure, the appropriate dimensions for the S-shaped damper were determined, and the nonlinear models of its finite elements were analyzed using cyclic loading to determine the hysteresis curve. The extracted curves were then used to examine the structures retrofitted with this damper through nonlinear time-history analysis. Finally, these retrofitted structures were compared with structures without dampers in terms of

various seismic characteristics to determine the effectiveness of this type of damper under different seismic conditions.

2. Modeling

2.1 Geometry and Loading of Studied Structures

In this research, three structures with heights of 4, 8, and 12 stories have been investigated. These structures are made of steel and have a symmetrical configuration. The span and width of the plan are made up of three 6m frames, respectively. The buildings are deemed to be 3 meters high. Therefore, the combined height of the structures is 12 m, 24 m, and 36 m, respectively. Fig. 1 illustrates the configuration of the studied structures and the nonlinear models developed for 4-, 8-, and 12-story structures based on this configuration.

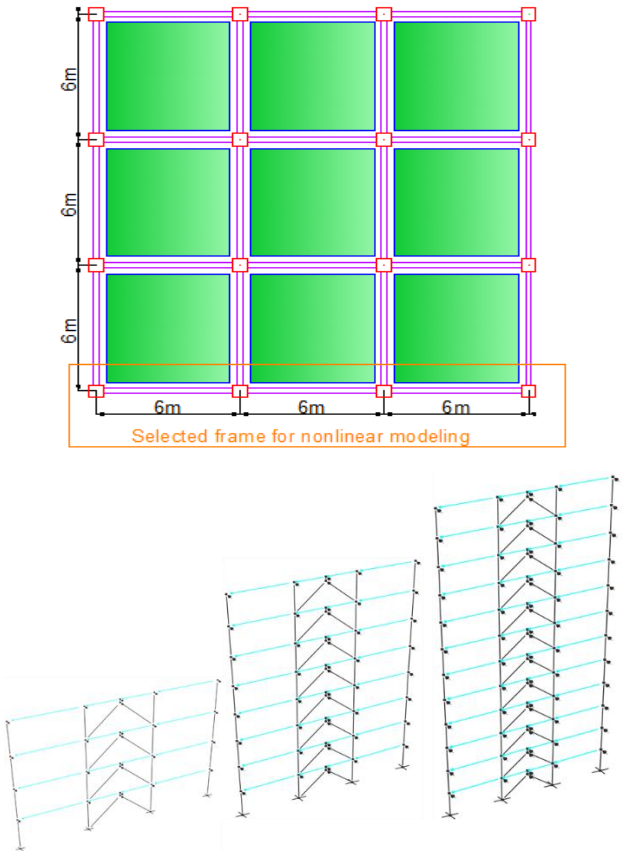

Fig. 1: Configuration of the selected Structure and the modeled frame with SSPD for modeling

The intended use of the structures is considered residential, so the structures' loads, according to this application, include dead, live, and snow loads. The dead loads, including the ceiling load, are equal to 5 kN/m^2, and the load due to external walls is equal to 7.5 kN/m^2. The live load of the story is 3 kN/m^2 and the snow load on the roof of the structure is 6 kN/m^2. According to the structure's configuration, a one-bay deck has been used to model the roof of the stories. This deck evenly distributes the load between the load-carrying paths and provides sufficient rigidity as a diaphragm against lateral loads.

The ASCE 7-17 code and the relevant design spectrum for severe seismicity have been considered for seismic loading (American Society of Civil Engineers, 2017). Drawing on this, the structure's seismic coefficient is determined according to its height and configuration, while the lateral load on each floor is calculated based on its seismic mass. Since the structure's geometry and loading are symmetrical, the center of mass and stiffness are aligned, and the earthquake-induced side loads are deployed, conforming to the ASCE code.

2.2 Linear Design of the Structure

Structures have been designed using linear analysis based on gravity and seismic loading. The design utilized the load combinations specified in the AISC 360-16 code, based on the type of steel structure (American Institute of Steel Construction, 2016). Additionally, P-Δ analyses were applied to enhance the moment of the members following the moment frame structural system. It should be noted that beams with broad flange sections that satisfy the seismic compactness conditions were used for beams, and box sections with similar conditions were used for columns. Finally, based on different loading conditions, the final result of selected sections for various classes of modeled structures is shown in Table 1.

2.3 Designing the Nonlinear Requirement of S-Shape Damper

The damper used in this study is an SSPD (Hibbitt et al., 2022). This damper is made by changing the shape of 2 flat plates through cold rolling and is connected to other structural members using bolts at both ends. Fig. 2 displays its general characteristics.

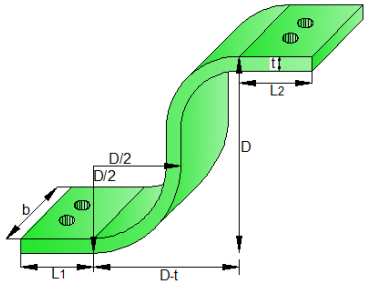

Fig. 2: Geometric characteristics of the S-shape damper (Federal Emergency Management Agency, 2007)

According to the provided geometry of the damper, the main specifications include the width of the damper (b), the thickness of the damper plate (t), and the diameter of the damper (D). Furthermore, the lengths of the first and last sheets, which are expressed as L1 and L2, respectively, play a decisive role in connection characteristics between the damper and structure (CSI, 2021). Based on these specifications, the damper's nonlinear behavior, geometric, and force-displacement, is illustrated in Fig. 3. Considering these conditions, the desired damper is designed according to equations 1 to 7.

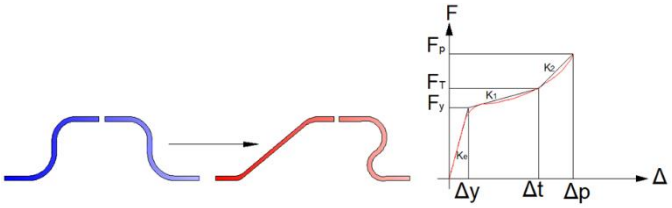

Fig. 3: Geometric nonlinear behavior and force-displacement of the S-shaped damper (Gholami et al., 2013)

Table 1: Sections of structures

story	4 story Beam (I) b_fXhXt_fXt_w(mm)	Column (box) (mm)	8 story Beam (I) b_fXhXt_fXt_w(mm)	Column (box) (mm)	12 story Beam (I) b_fXhXt_fXt_w(mm)	Column (box) (mm)
1	240X240X17X10	240X240X20	300X300X11X19	320X320X20	340X340X21.5X12	360X360X30
2	240X240X17X10	240X240X20	300X300X11X19	20X320X20	340X340X21.5X12	360X360X30
3	220X220X16X9.5	200X200X16	280X280X18X10.5	280X280X28	320X320X20.5X11.5	320X320X30
4	220X220X16X9.5	200X200X16	280X280X18X10.5	280X280X28	320X320X20.5X11.5	320X320X30
5	-	-	260X260X17.5X10	260X260X18	300X300X11X19	320X320X30
6	-	-	260X260X17.5X10	260X260X18	300X300X11X19	320X320X30
7	-	-	220X220X16X9.5	240X240X20	280X280X18X10.5	280X280X20
8	-	-	220X220X16X9.5	240X240X20	280X280X18X10.5	280X280X20
9	-	-	-	-	260X260X17.5X10	280X280X20
10	-	-	-	-	260X260X17.5X10	280X280X20
11	-	-	-	-	240X240X17X10	240X240X20
12	-	-	-	-	240X240X17X10	240X240X20

$$K_e = 2.39Eb\left(\frac{D}{t}-1\right)^{-2.63} \quad (1)$$

$$\Delta_y = 1.94\frac{f_y t}{E}\left(\frac{D}{t}-1\right)^{1.58} \quad (2)$$

$$F_y = K_e.\Delta_y \quad (3)$$

$$K_1 = 0.001K_e\left(\frac{D}{t}\right)^{1.5} \quad (4)$$

$$K_2 = 10^{-5}\times 5.97K_e\left(\frac{D}{t}\right)^{2.88} \quad (5)$$

$$F_p = 0.96f_y bt \quad (6)$$

$$\Delta_p = 163.38\Delta_y\left(\frac{D}{t}\right)^{-1.05} \quad (7)$$

Based on Fig. 3, the key mechanical properties of the damper, including the initial stiffness (Ke), yield displacement (Δy), yield force (Fy), post-yield (secondary) stiffness

(k1), rehardening stiffness (k2), ultimate force capacity (Fp), and equivalent displacement (Δp), are clearly identified.

According to these equations and based on the shear demand of the story obtained from the linear static analysis, the dimensions of the damper are determined as shown in Table 2. The design ensures that the story's shear force exceeds the damper's yield force but remains between 40% and 70% of the final force, guaranteeing its ductile performance.

Table 2: Properties of dampers

	t	k_e	K_1	K_2	F_y	F_t	F_p
4 story							
	mm	kN/mm	kN/mm	kN/mm	kN	kN	kN
4	10	43	4	17	101	202	461
3	14	11	6	15	206	387	645
2	18	228	8	14	353	634	829
1	20	310	10	13	443	782	922
8 story							
	t	k_e	K_1	K_2	F_y	F_t	F_p
	mm	kN/mm	kN/mm	kN/mm	kN	kN	kN
8	6	4	1	26	22	51	276
7	12	24	3	25	95	197	553
6	16	52	4	22	174	343	737
5	20	97	6	22	279	529	922
4	24	163	7	20	411	755	1106
3	26	205	8	18	488	883	1198
2	28	254	9	16	573	1022	1290
1	30	310	10	15	665	1173	1382
12 story							
	t	k_e	K_1	K_2	F_y	F_t	F_p
	mm	kN/mm	kN/mm	kN/mm	kN	kN	kN
12	6	2	1	22	21	48	346
11	10	8	2	20	59	133	576
10	12	13	3	20	87	189	691
9	14	20	3	19	120	254	806
8	16	29	4	19	158	329	922
7	18	41	4	18	203	412	1037
6	20	54	5	18	253	505	1152
5	22	71	5	18	309	607	1267
4	24	90	6	18	371	718	1382
3	26	113	7	18	440	839	1498
2	28	139	8	18	515	969	1613
1	30	169	8	18	597	1108	1728

In this process, the diameter of the damper design for 4-, 8-, and 12-story structures is considered 200, 300, and 400 mm, respectively. Additionally, the width of the damper for 4-, 8-, and 12-story structures is specified as 200 mm, 200 mm, and 250 mm, respectively.

2.4 Nonlinear Finite Element Modeling

This article discusses the effectiveness of the S-shaped damper. Because the nonlinear characteristics of a damper have a strong influence on the overall performance behavior of the structure, it is important to model them accurately. Achieving this level of precision is not possible solely through the relations provided. Therefore, the dampers designed in Segment 3.2 were simulated and reviewed using the finite element method to extract their nonlinear behavior and ensure their seismic performance more accurately.

Finite element modeling was conducted using ABAQUS 2022 software. One of its key features is its capability to model the nonlinear behavior of metal materials under various conditions and to control geometric nonlinear effects, making it ideal for control system modeling (Hibbitt et al., 2022).

Modeling the behavior of steel elements and materials

Since the S-shaped damper is attached to the structure using bolts, according to Zhai's research (Zhai et al., 2020), its effects should be considered in the modeling. According to Table 3, two types of steel were used to model the damper and bolts.

Table 3: Properties of the damper's steel

Steel type	E (Elastic module (MPa))	ϑ (poison ratio)	f_y (MPa)	F_u (MPa)	Elongation (%)
Damper	210000	0.3	260	330	27
Bolt	300000	0.3	660	830	15

Given that the nonlinear behavior of the damper is directly influenced by the stress-strain curve of the damper material, the curve used in modeling the damper steel is based on the curve presented in the study by Zhai et al. (Fig. 4) (Zhai et al., 2020).

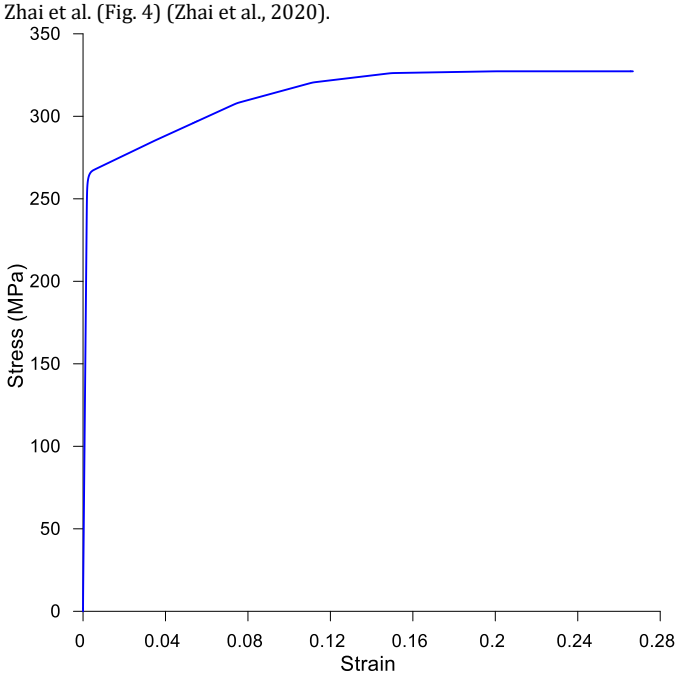

Fig. 4: Stress-strain curve of the steel used in the construction of the arched part of the damper

It should be noted that the steel specifications provided for the damper are based on research by Zhai et al., where combined hardening was deployed to replicate the actions of the damper's steel (Zhai et al., 2020). This hardening approach enables modeling of both isotropic and kinematic hardening, where the yield surfaces expand and shift (Hibbitt et al., 2022).

C3D8R elements are used for meshing and damper configuration. These elements are solid, 8-sided cubes with one node at each corner. Three angular and three lateral directions are available for each node. Additionally, these elements enable modeling geometric nonlinear behavior and plastic deformation, particularly in the component's depth, thereby allowing more accurate control over the damper's behavior in the models (Hibbitt et al., 2022). Fig. 5 displays the mesh applied to the 4t-2 model. It should be noted that '4t-2' refers to the damper used in a 4-story structure on the second story.

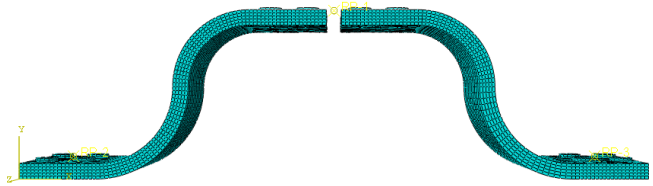

Fig. 5: Mesh implemented on the finite element model of 4t-2

Geometric configuration, boundary conditions, and loading

The sizes of the modeled dampers are determined from Table 2. Since the damper is connected using bolts, four bolts are used at the upper part and four bolts at the lower part of each damper to transfer the shear force between the damper and bolts linearly.

Hard contact and frictional sliding were used to represent the interaction between the bolts and the damper. The hard contact formulation was used to describe surfaces with varying surface conditions and to account for the potential separation or non-separation of the two

surfaces following impact. In the model, the location and probability of separation were determined based on the mechanical behavior of the same steel that composes both bolts and the damper (Hibbitt et al., 2022).

Since the passage of forces from the damper to the main structural body is controlled mainly by the inherent stiffness in the bolt–damper assembly, the friction effect is negligible in this mechanism. Accordingly, a friction coefficient of 0.1, together with a force decay condition, was assigned for this interface (Hibbitt et al., 2022).

Furthermore, consistent with the findings reported by Zhai et al., the bolts primarily function in a supporting capacity; therefore, no specific prestressing force was applied to them in the model (Zhai et al., 2020).

Boundary loading and displacement control conditions are applied based on Zhai's research (Zhai et al., 2020) for the upper bolts and the end plates, with the stability of the lower part assumed and displacement control applied to the upper part, as per Federal Emergency Management Agency Publication 461 (FEMA-461) regulations. Fig. 6 displays the loading history for the 4-story dampers and the boundary conditions used in the finite element modeling (Federal Emergency Management Agency, 2007).

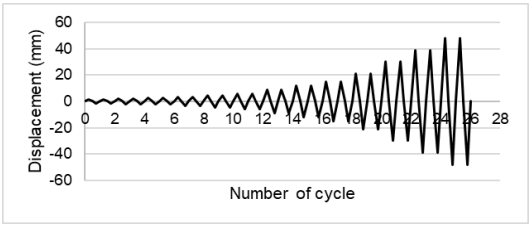

(a)

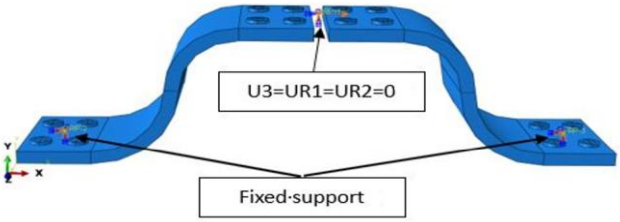

(b)

Fig. 6: Boundary conditions applied to the structure: a) Loading history of the 4-story utilized dampers, b) Support conditions

Verification of finite elements

To ensure the correctness of the method used in this part, laboratory sample S8 was selected from Zhai's research (Zhai et al., 2020). Its finite element model was analyzed using cyclic nonlinear loading and compared with the test results in Fig. 7. As illustrated, there is a strong correlation between the outcomes obtained from the nonlinear finite element analysis and the experimental results.

Fig. 8 presents a comparison between the deformations observed in the experimental damper by Zhai et al. and those predicted using the validated FEM at its initiation and termination of loading cycles (Zhai et al., 2020).

As illustrated in Fig. 8, the finite element model accurately captures the deformation observed in the original specimen across the various stages of loading.

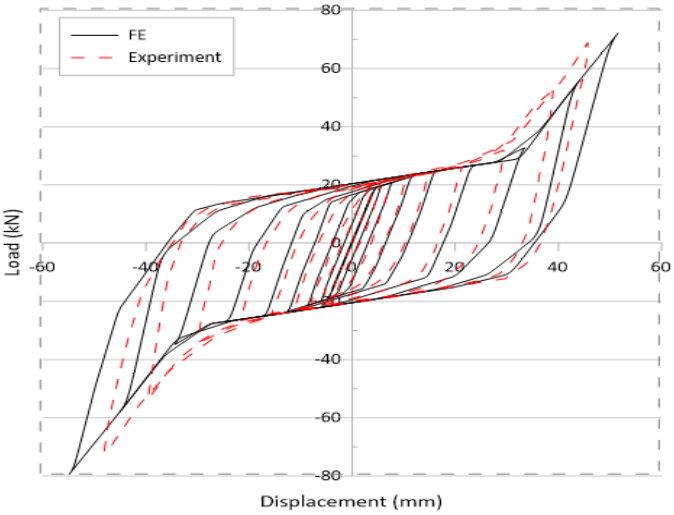

Fig. 7: Comparison between outcomes and finite elements

2.5 Nonlinear Modeling of Structures

Configuring nonlinear models

This article thoroughly examines the connection configuration in the modeling, given that the impact of incorporating an S-shaped damper into the steel moment frame has been studied. In view of the damper geometry and detailing, ideal positioning would be between the chevron brace and its top beam, tied with stiffened bolts.

PERFORM V.8 software has been used for nonlinear modeling, as it provides the capability to model the nonlinear behavior of various structural elements for both static and dynamic analysis (CSI, 2021). Fig. 9 displays the details of the nonlinear modeling, highlighting the selective elements for the frame members and the connection system of the S-shaped damper to the frame.

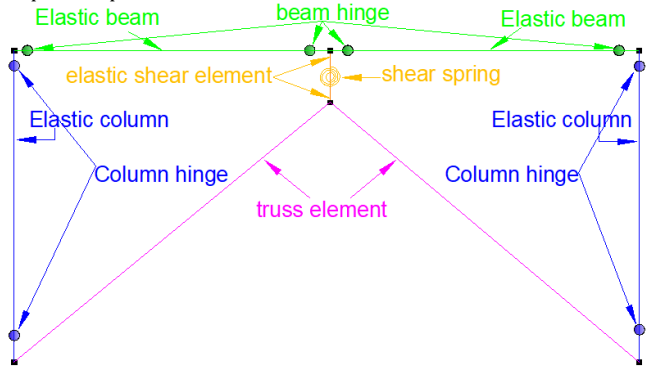

Fig. 9: Configuration of the model developed in the software based on the proposed geometry of the damper connection to the structure

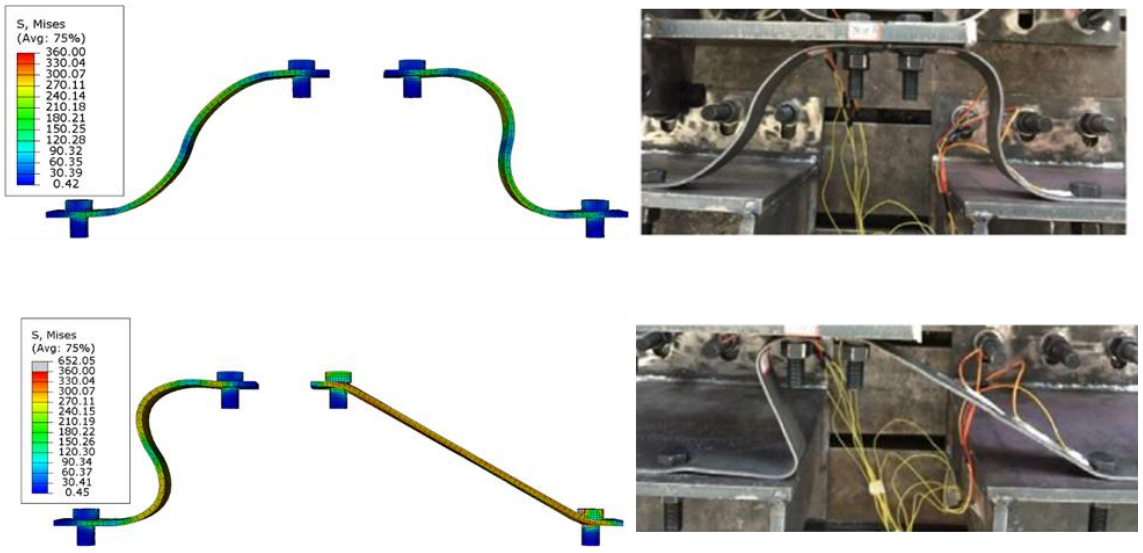

Fig. 8: Comparison of the deformation in the finite element model compared to the original verified specimens at the beginning and end of the loading cycles

It should be noted that the nonlinear hinges of beams and columns are of the concentrated plastic type, which can account for the loss of strength and degradation of stiffness based on energy models. Furthermore, column hinges can simulate effects of axial force while bending moment due to the P-Δ effect, so that their performance can be closely matched with actuality for real situations. The vibration behavior is controlled by the linear method of Newton, wherein a time step of 0.05 s was applied. Finally, a damping ratio of 5% is used for all vibration conditions (CSI, 2021).

Verification of nonlinear modeling

Considering that the main structure investigated in this research is a medium steel moment frame, a laboratory sample from the study by (Gholami et al., 2013), which focused on a beam-to-column connection in a steel bending frame that includes an I-shaped beam and a box column, is used. The connection has been analyzed under cyclic loading conditions. The selected connection is an exterior joint, which comprises a 2500 mm long column and a beam spread out along both sides of the column, with a total length of 3000 mm. Fig. 10 shows the geometric details corresponding to the laboratory model and the nonlinear model created in the Perform software.

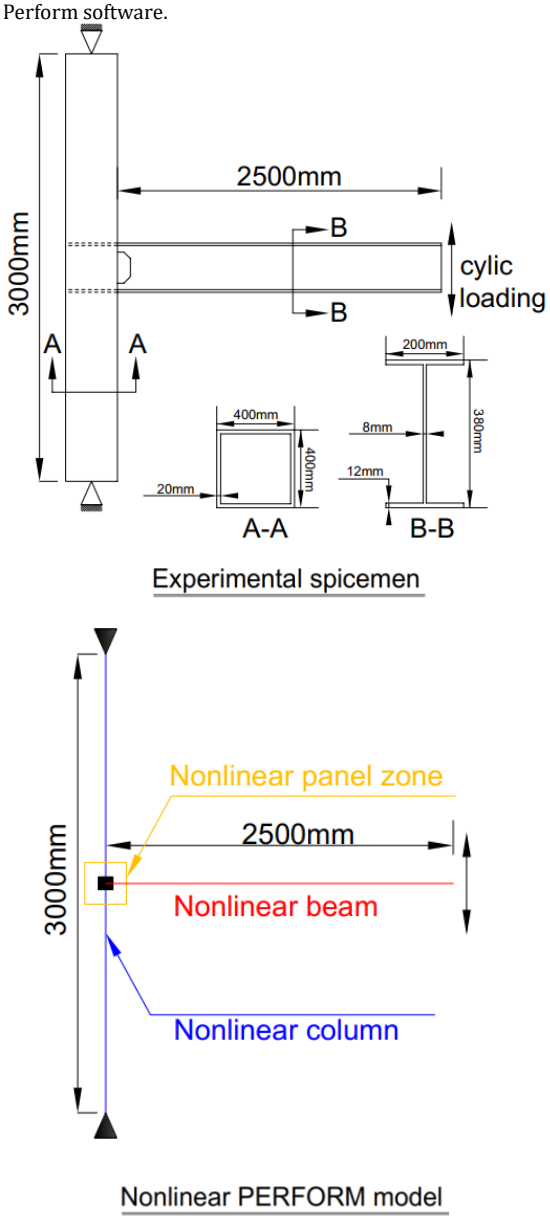

Fig. 10: Geometric details corresponding to the verified moment frame connection laboratory specimen and the nonlinear model in PERFORM

The desired connection is subjected to cyclic loading, and its hysteresis behavior is determined. Fig. 11 displays the outcomes of the modeling and the laboratory sample. The red curves in the figure are actually the push-hysteresis curves used to calculate the stiffness, yield strength, and ultimate strength.

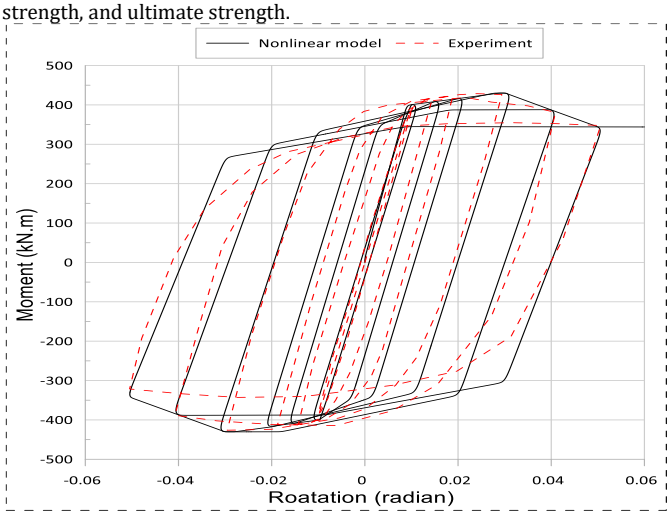

Fig. 11: Comparing the outcomes of the experiment and modeling of the connection of the beam to the column of the medium-moment steel frame

Selection of earthquake records and scaling

The selected earthquakes must have the appropriate characteristics to be applied to the structure. For this purpose, seven records of earthquakes far from the fault with D in seismicity conditions were selected to be applied to the structures. Table 4 displays selected records along with their corresponding seismic conditions.

In the next step, the records are scaled so that the average spectrum is not less than the shape spectrum of the design spectrum of the ASCE 7-17 code for seismicity category D at any point. Fig. 12 displays the comparison between these spectra (American Society of Civil Engineers, 2017).

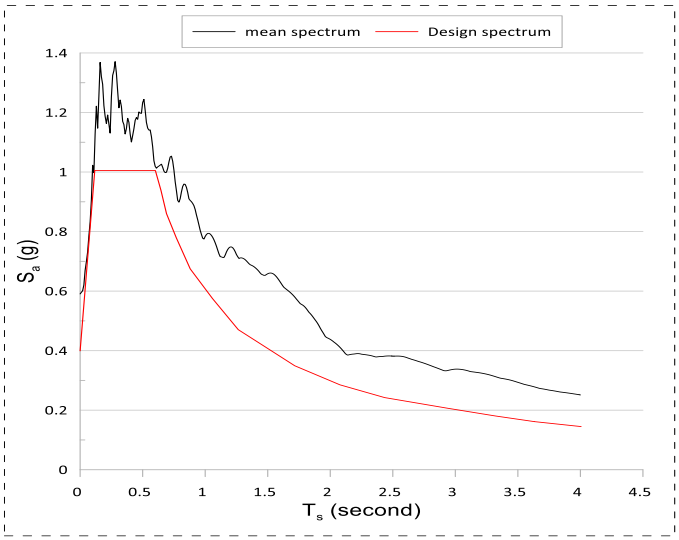

Fig. 12: Comparison of the mean spectrum of selected and designed records

Table 4: Records and seismic conditions

	Earthquake	Country	Year	Mech	Mag	Station	Rjb(km)	PGA	PGV
1	Kocaeli	Turkey	1999	Strike-slip	7.5	Duzce	13.6	0.31	117
2	Cape Mendocino	America	1992	Reverse	7	Rio Dell	7.9	0.32	49
3	Hector mine	America	1999	Strike-slip	7.1	Hector	10.35	0.328	44.77
4	Chi-chi	Taiwan	1999	Obilique	7.6	CHY101	9.94	0.34	65
5	Superstition hills	America	1987	Strike-slip	6.5	El Centro	18.54	0.35	48
6	Friuli	Italy	1976	Reverse	6.5	Tolmezzo	14.97	0.35	23
7	Imperial valley	America	1979	Strike-slip	6.5	Delta	22.03	0.35	33

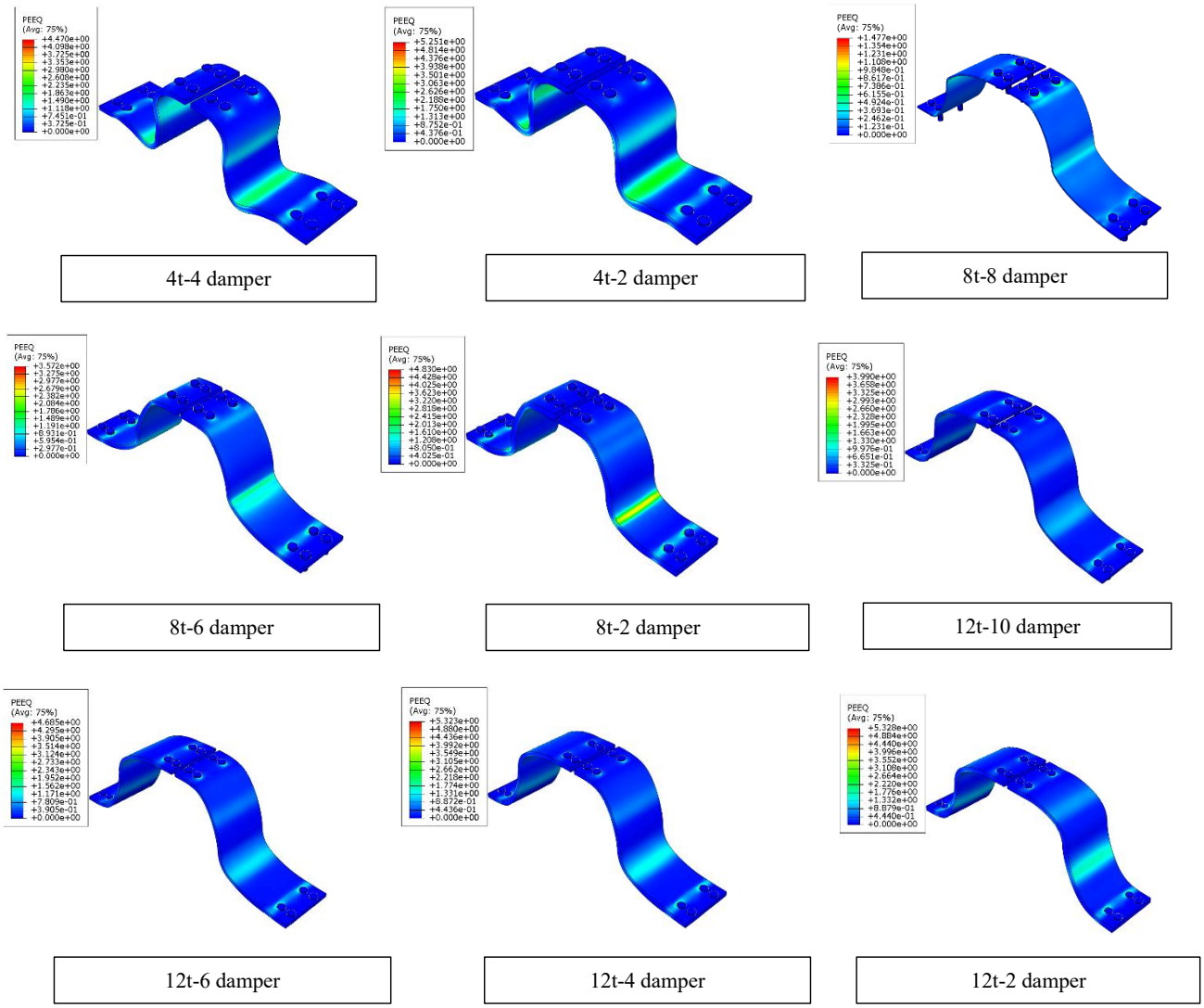

Fig. 13: Equivalent plastic strain created in several dampers under investigation in different floors of the studied structures

3. Outcomes and Discussion

3.1 Finite Element Outcomes

Deformation

Fig. 13 displays the deformation and plastic strain distribution of some models in the investigated dampers.

As shown in Fig. 13, as the structure's height increases, the force applied to the lower stories increases, and the damper bears more stress. In the 4-story structure, the damper located on the second floor bears a larger and more critical stress. Similarly, in the 8-story structure, the damper on the second floor bears more stress than the damper on the sixth and top floors, indicating a crucial area. In the 12-story structure, dampers on the second and fourth floors experience higher stress than those on the sixth and tenth floors. This means that the damping has less effect as the height of the structure increases.

Hysteresis behavior

The hysteresis behavior of the dampers is used to assess the productivity of materials under cyclic stress. This curve represents the nonlinear plan, energy absorbed, and therefore wear. The amount of energy absorbed in different stories is shown in Fig. 14.

The outcomes show that increasing the damper plate thickness significantly enhances yield and ultimate strength in all three structures' damper groups while noticeably reducing secondary hardening. The enclosed surface area in loading cycles also increases, indicating improved energy absorption capacity in floor dampers on the lower story. Additionally, as the damper diameter increases, strength decreases under similar conditions, as observed in dampers 8t-6 and 12t-8.

Stiffness

As depicted in Fig. 15, the stiffness of the damper in the lower story is reduced when compared with that of the upper story. This issue is due to sections with greater thickness and width on the lower story. In Fig. 12, for buildings with four stories, the stiffness of the damper on the first story exhibits a significant difference compared to the other stories, displaying 46%, 192%, and 760% more resistance than the second, third, and fourth stories, respectively. For an 8-story building, this difference is less. Thus, the first floor is stiffer than the second, fourth, and eighth floors, with factors of 9%, 109%, and 1550%. For a URM L12 building, the ratio of stiffness of the first floor to the second, fourth, sixth, and tenth floors is (22%, 86%, 297%,846 %). Meanwhile, the stiffness of the first floor of a 4-story building is equal to 121% and 170% of that of 8- and 12-story buildings, respectively. This issue can be attributed to the better performance of the S-shaped damper for shorter buildings. In other words, in the 4-roof building, smaller sections have been used, and the damper has been more adapted to the use of the structure to boost the nonlinear behavior.

Yield strength and ultimate strength

The yield strength of the dampers in different buildings and their stories is shown in Fig. 16. In the 4-, 8-, and 12-story buildings, the yield forces are 280, 355, and 360 kN, respectively. The damper in the 4-story building experiences a lower yield force at lower levels compared to the damper in the 8- and 12-story buildings. However, this trend reverses on the upper stories, with the 4-story building showing more than four times the yield strength compared to the 8- and 12-story buildings.

The ultimate force imposed on the damper in Fig. 17 is similar to the yield force. The difference is that, unlike the maximum yield force, the ultimate force in the 12-story building is 21% higher than in the 8-story building and 83% higher than in the 4-story building. Additionally, the ultimate force distribution for all three buildings is nearly linear. This is due to the damper's effective energy dissipation.

3.2 Outcomes of Nonlinear Analysis

Pushover analysis and bilinear curves

Fig. 18 shows the curves resulting from the pushover analysis of structures with and without dampers, for different numbers of stories.

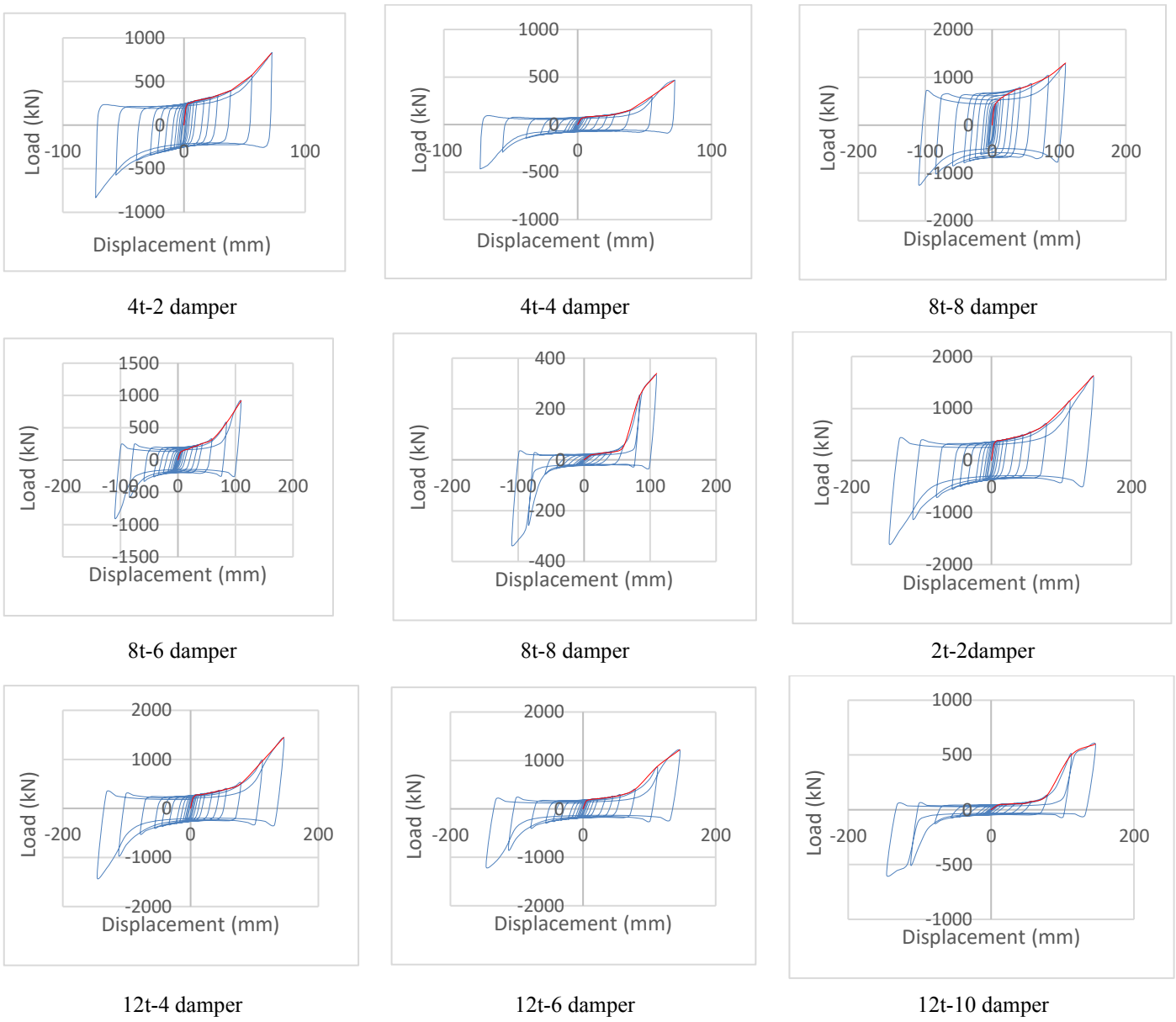

Fig. 14: Hysteresis curve of some FEM-modeled dampers

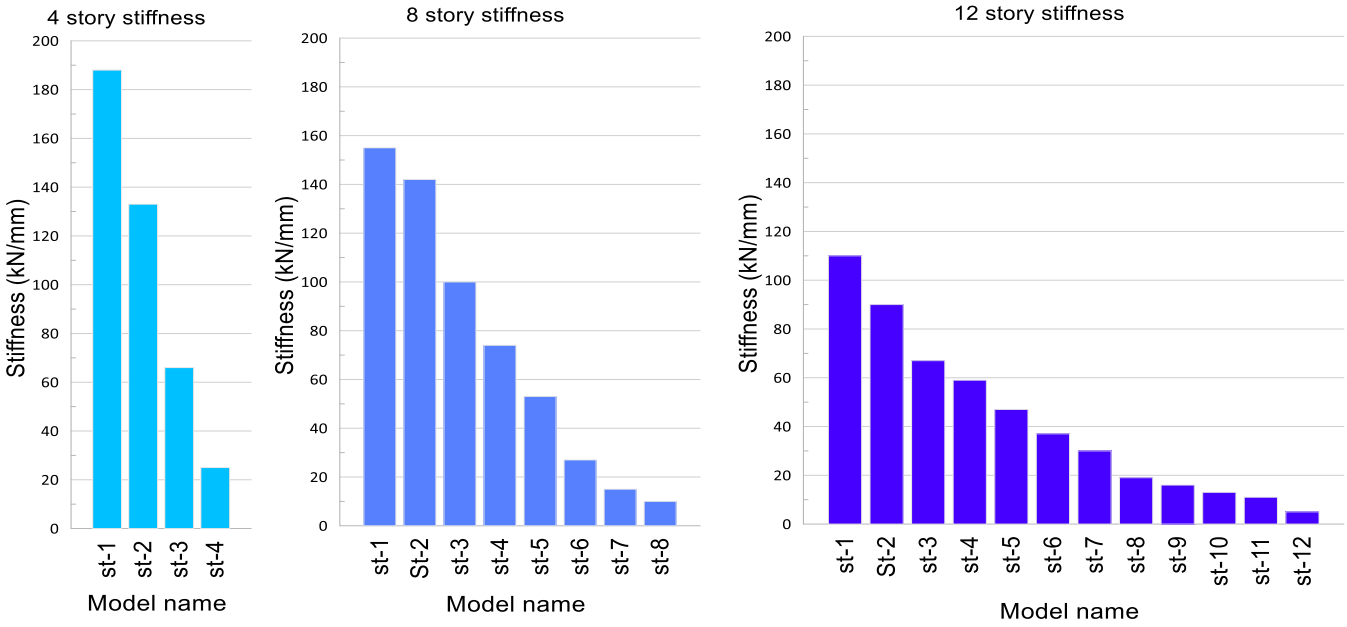

Fig. 15: Stiffness of FEM-modeled dampers

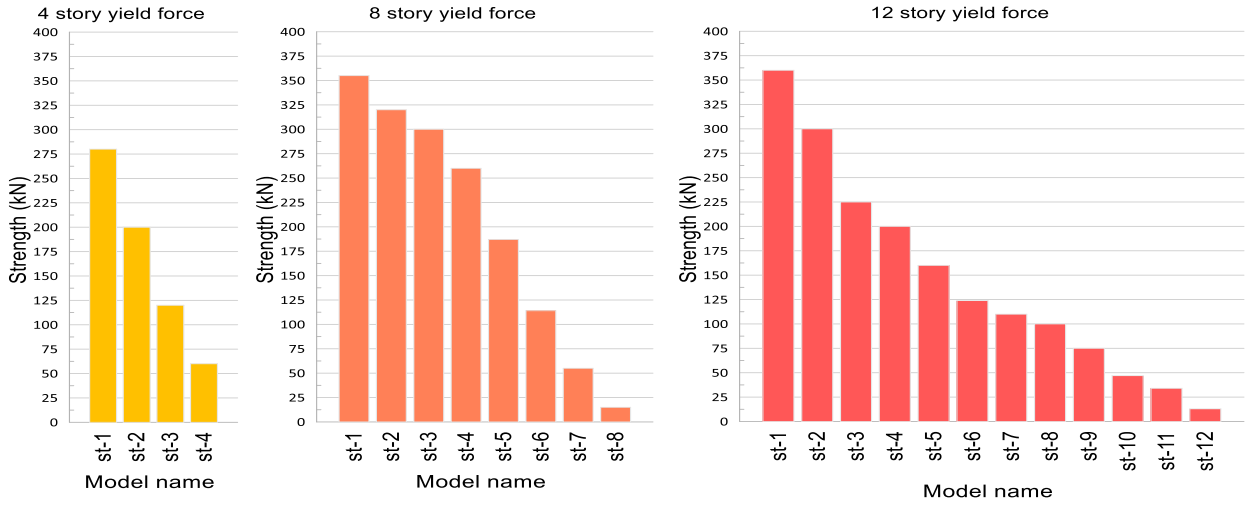

Fig. 16: Yield strength of FEM-modeled dampers

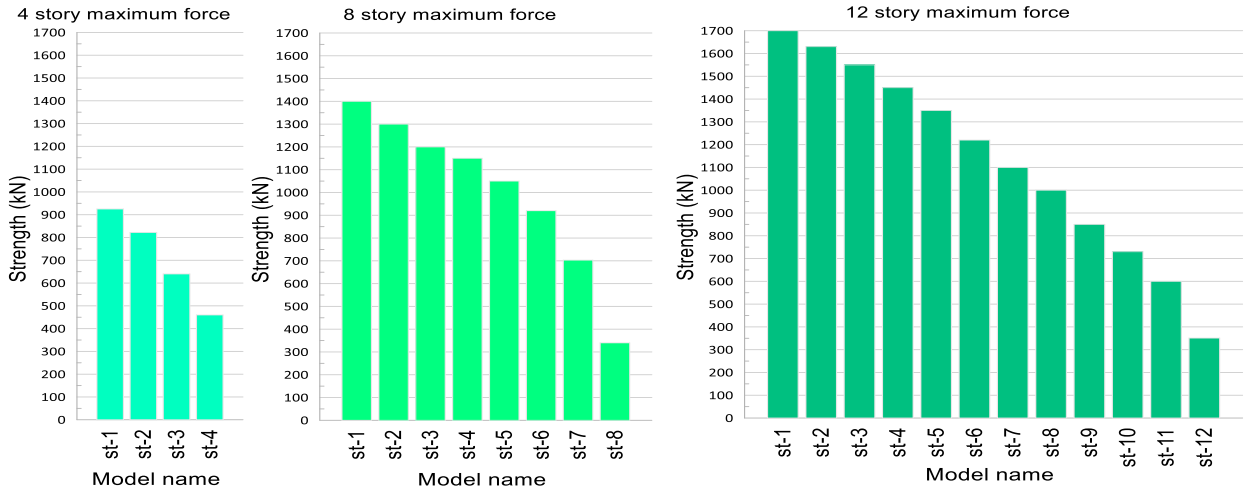

Fig. 17: Ultimate strength of FEM-modeled dampers

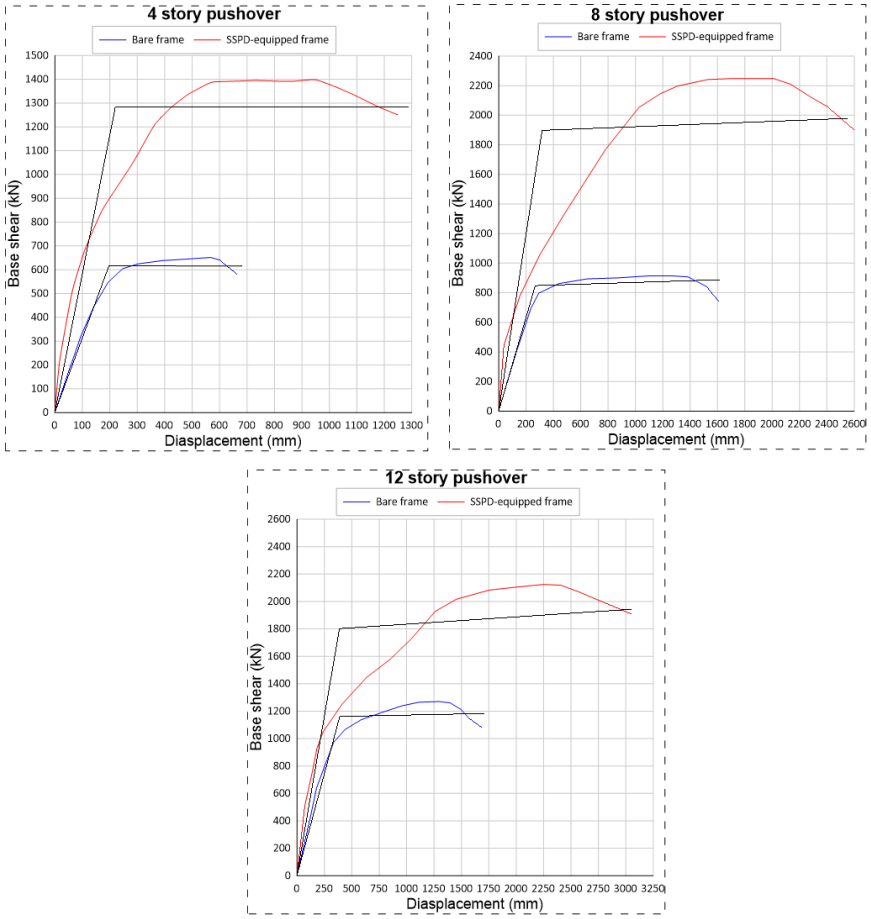

Fig. 18: Pushover curve of analyzed structures

Contrary to the similarity in the behavior of the pushover curves for the 4-, 8-, and 12-story buildings, the values of the pushover and bilinear curves are not identical. It is clear from Fig. 15 that the damping effect has increased the pushover values by 109%, 123%, and 51% for the 4-storey, 8-storey, and 12-storey buildings, respectively. For the 4-story building, regardless of the damper's effect, the yield and ultimate forces derived from the bilinear diagram are 614.7 kN, 652 kN, 1279.9 kN, and 1398.1 kN, respectively. For the 8-story building, the yield and ultimate strengths estimated from the bilinear diagram are 861.7 kN, 913.6 kN, 1956.9 kN, and 2248.4 kN, respectively. Finally, for the 12-story building, the yield and ultimate strengths estimated from the bilinear diagram are 1,193.4 kN, 1,270.6 kN, 1,828.7 kN, and 2,124.4 kN, respectively. The presence of the damper has increased the area under the curve, absorbing more energy, which indicates the damper's effectiveness and potential. In the 4- and 8-story buildings, the damper has doubled the curve area; in the 12-story building, this increase is about 60%. This suggests that as the structure's height increases, the effect of the damper decreases, which can be observed in the 8- and 12-story buildings.

Higher structures induce more displacement, both with and without dampers. For the 4-story building, the maximum displacement with and without the damper is 1256 mm and 663 mm, respectively. For the 8- and 12-story buildings, the maximum displacements with and without dampers are 2,600 mm, 1,611 mm, 3,049 mm, and 1,686 mm, respectively. The displacement rises as the structure's height increases. The damper has increased the structure's capacity and extended its nonlinear behavior beyond the point where the bare frames reach their ultimate strength. Thus, using a damper in the 4-, 8-, and 12-story structures results in larger displacements by 90%, 61%, and 80%, respectively.

Base shear

The highest base shear recorded in the 4-story structure without a damper during the Rio Dell earthquake is 949 kN. In comparison, the maximum base shear during the Duzce earthquake is 2341 kN for the case with a damper. The 8- and 12-story structures experience the maximum base shear during the Duzce earthquake. In that order, the base shear values for the bare frame with SSPD are 1,396 kN, 2,397 kN, 1,935 kN, and 2,787 kN. These outcomes show an increase of 146%, 171%, and 144% for the 4-, 8-, and 12-story buildings, respectively. The outcomes reveal a 146%, 171%, and 144% rise for 4-, 8-, and 12 structures, respectively. Therefore, buildings with SSPD experience a higher base shear. The maximum base shear for all buildings equipped with a damper is similar. Additionally, the average value of this measure is approximately 1900 kN. Thus, buildings with SSPD experience a higher base shear. Notably, the maximum base shear for all buildings with dampers is similar, with the average value being approximately 1900 kN.

According to Fig. 19, for buildings 4 and 8, the base shear without a damper is nearly the same, and after adding the damper, their measures become different. It can refer to recording differences so that values do not follow a specific pattern. Additionally, for these structures, after utilizing SSPD, the base shear increases significantly. However, this subject does not apply to a 12-story structure. For 12-story buildings, SSPD does not reveal a sound effect, even for a few samples that have seen a base shear drop. This problem can refer to a decrease in the damper effect for high-rise structures.

Maximum displacement

According to Fig. 20, the maximum displacements of 4-, 8-, and 12-story buildings with a damper are 314.7, 525, and 719 kN, respectively. These values for bare structures are 485, 898, and 984 kN, respectively. So, 4-, 8-, and 12-story structures without dampers experienced maximum displacements of 54%, 71%, and 36%, respectively, higher than those of bare buildings.

The average maximum displacement of 8 and 12 stories with SSPD is similar, contrary to that of 4 stories. This subject refers to reducing the damper effect along the height of the structure. 4-story structures with SSPD have experienced a decline in average maximum displacement of about 55%. For 8- and 12-story buildings, these reductions are approximately 40% and 30%, respectively. This behavior reveals the suitable effect of the damper.

Inter-story drift

The drift behavior of all structures is nonlinear. Fig. 21 illustrates that taller buildings exhibit more pronounced nonlinear behavior. In the uninfilled 4-, 8-, and 12-storey frame buildings, the interstory drift maxima were found to be approximately 0.046 for the third story, 0.048 for the second story, and nearly 0.05 for the fourth story. The highest lateral drift observed in the 4-, 8-, and 12-story buildings with dampers was equal to 0.019 (at story #2), 0.025 (at story #5), and 0.019 (at story #7), respectively. Therefore, the damper resulted in decreases of 41%, 54%, and 38% in drift for the cases of 4-, 8-, and 12-story buildings, respectively. Additionally, the presence of the damper shifted the maximum drift to higher stories.

On average, the presence of the damper resulted in a constant drift value of approximately 0.014. This indicates that the damper has made the structure's response more uniform and significantly reduced the drift values. As mentioned, the damper has shifted the maximum drift to higher stories. The maximum drift averages for the bare frame are 0.026, 0.024, and 0.022 for stories 4, 5, and 6, respectively. For the structures with SSPD, these values are 0.012, 0.014, and 0.014 on stories 2, 5, and 9, respectively.

Energy

Based on Fig. 22, the maximum dissipated energy of the bare frame for 4-, 8-, and 12-story buildings is 649, 980, and 2392 kJ, respectively. Regarding these values, the maximum dissipated energy in proportion to the structure's height has increased. The maximum dissipated energy of the frame with a damper for 4-, 8-, and 12-story frames is 1056, 1410, and 2585 kJ. As is visible, the presence of a damper has led to an increase of dissipated energy in the amounts of 62%, 43%, and 8%, respectively. As in the last section, increasing the structure's height reduces the damper effect.

The damper's maximum dissipated energy has the same trend as the frame with the damper. Maximum dissipated energy of 4-, 8-, and 12-story buildings with a damper is 1041, 1320, and 2227 kJ. Based on these outcomes, it can be inferred that a damper dissipates most of the frame energy and has a significant impact on the structure's behavior. In 4-story, 8-story, and 12-story dampers, energy is dissipated in amounts of 93%, 86%, and 79%. So, frames with BSD have maximum dissipated energy and reveal the significant effect of the damper on the structure.

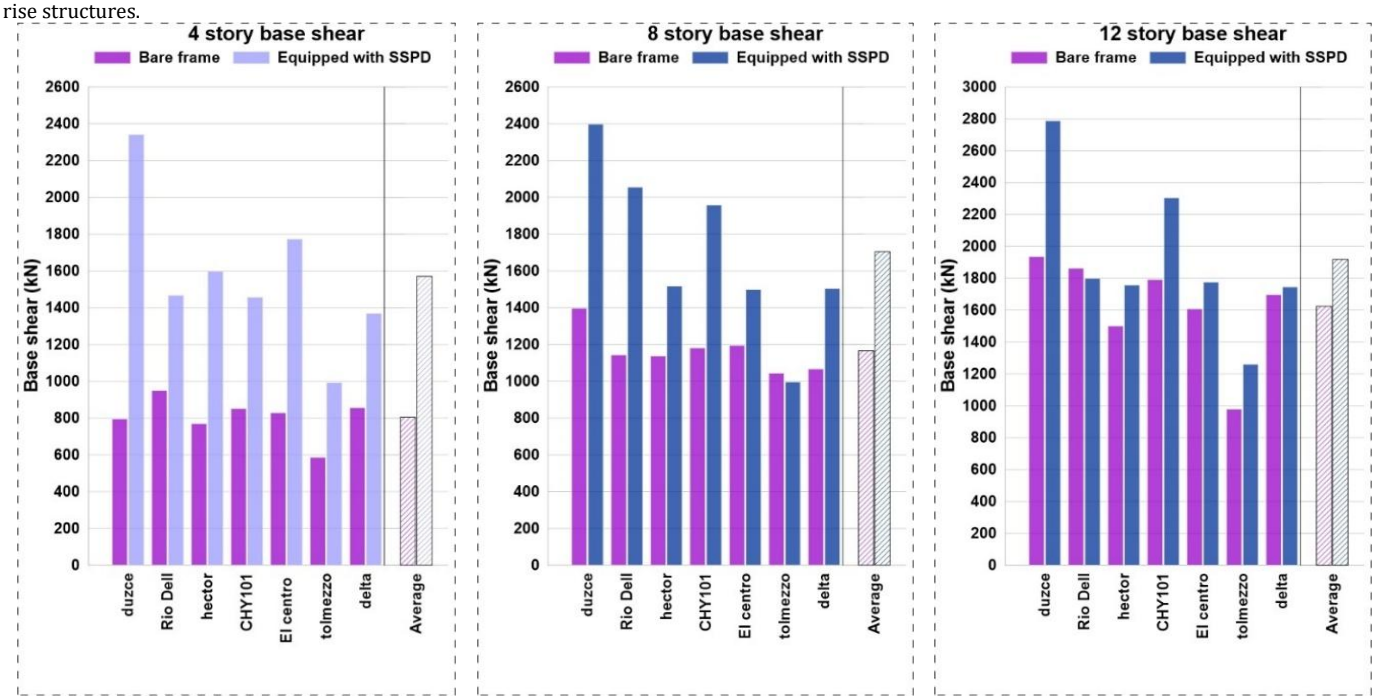

Fig. 19: Base shear of structures

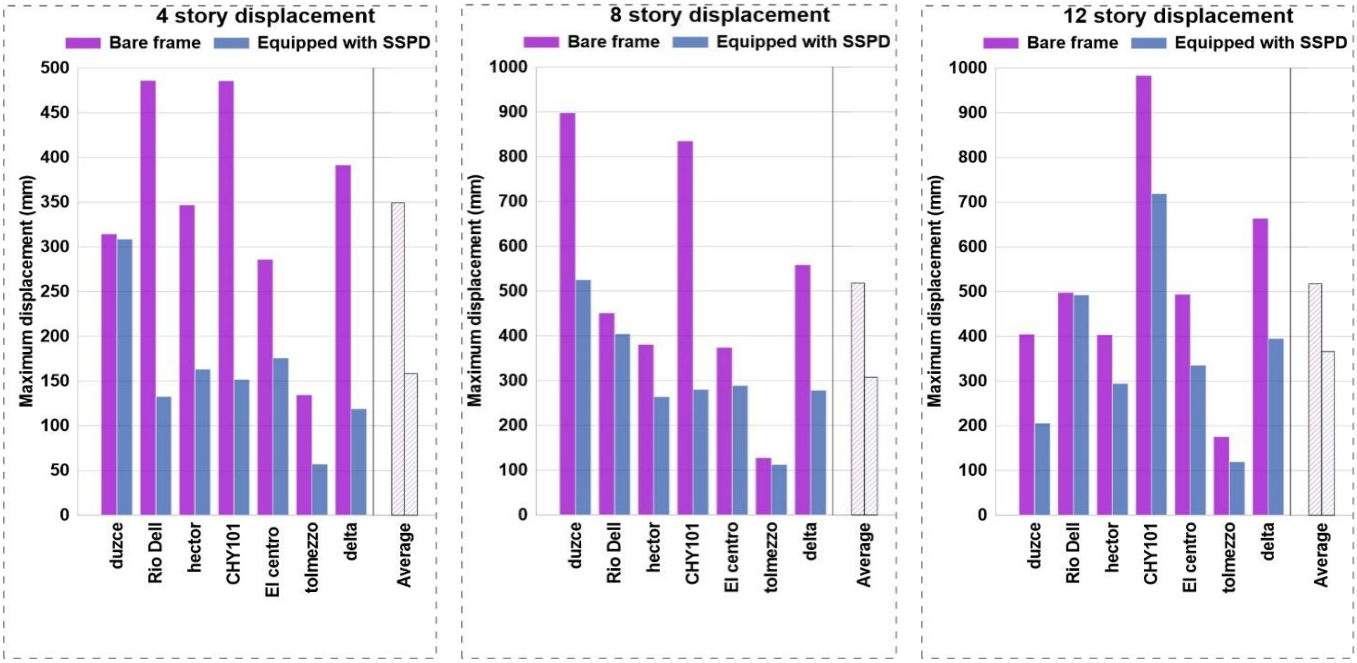

Fig. 20: Displacement of structures

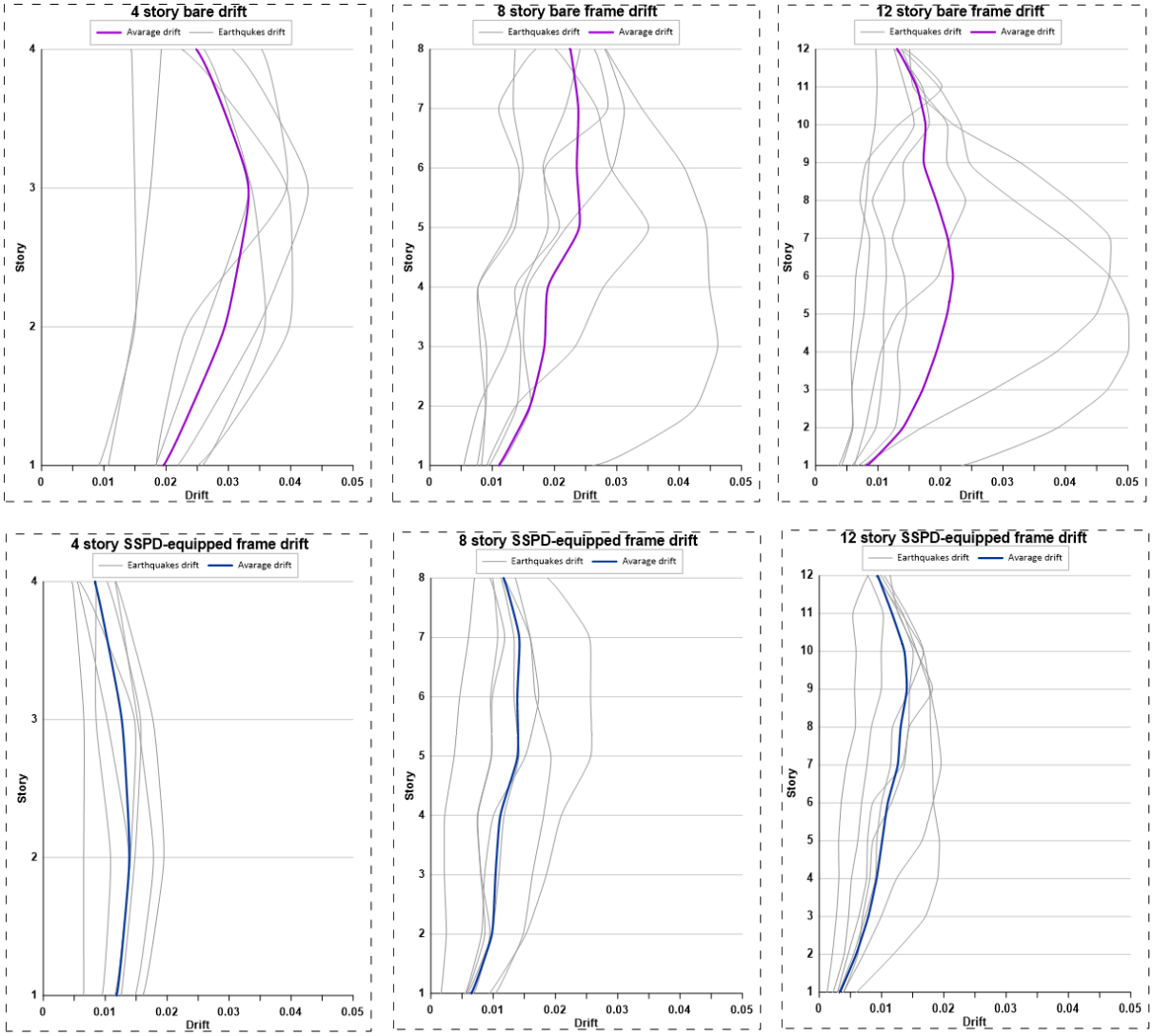

Fig. 21: Drift of the studied structure

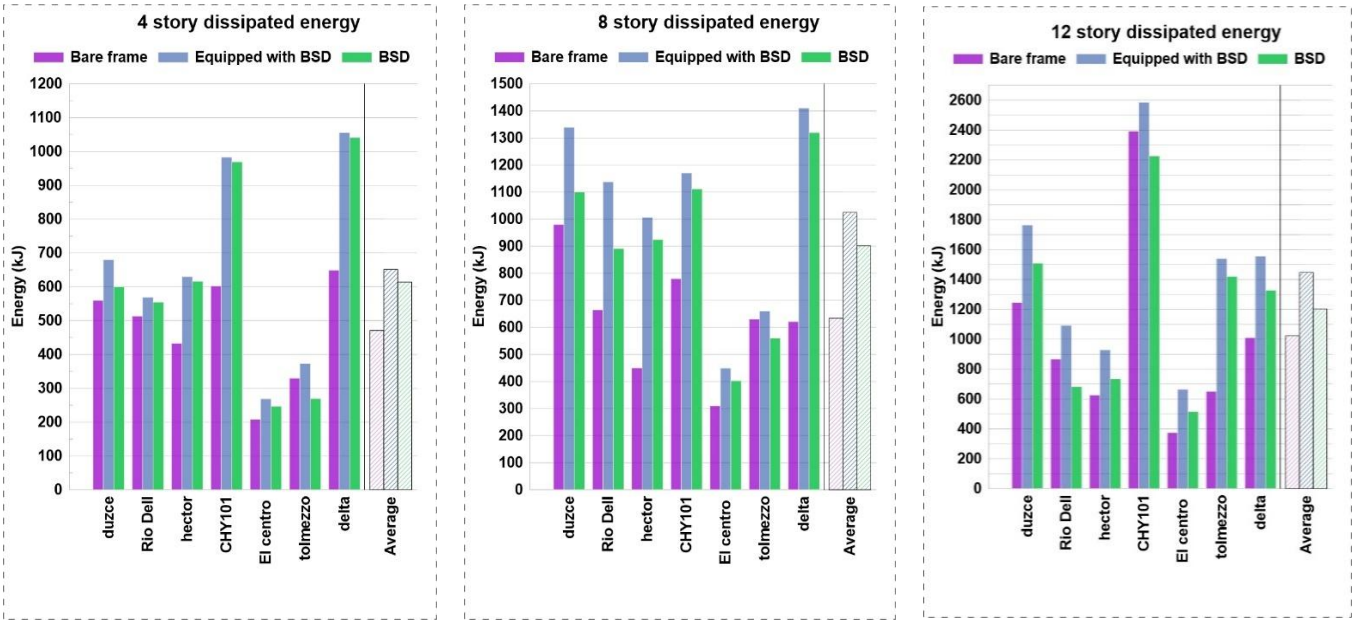

Fig. 22: Dissipated energy of structures

4. Conclusion

This research investigates the seismic characteristics of steel MRFs with S-shaped yielding dampers in comparison to those without them. The study involved subjecting three frames, with and without dampers, to seven earthquake records of varying intensities. The outcomes of the nonlinear analysis show the following:

1. The stiffness of the damper in the lower stories is lower than in the higher stories. This can be attributed to the greater thickness and width of the damper section in the lower stories.
2. The existence of the damper has expanded the floor area under the pushover curve, which results in more dissipating energy. The areas are doubled for the 4-story and 8-story buildings, while that of the 12-story building is approximately 60% larger. Furthermore, the greater dissipated energy allows for an increase in the levels of the structure. As observed with displacement and drift histories, the dissipated energy also grows with the height of the structure; however, at a decreasing rate as the height increases.
3. The average maximum displacements of 8 and 12 stories with SSPD are close to each other, unlike those of four stories. This issue refers to reducing the damper effect along the structure's height. Additionally, the increase in the structure's height has resulted in a more nonlinear behavior of the drift diagram, shifting the maximum drift to a higher story.
4. The maximum inelastic energy of the 4-story, 8-story, and 12-story damped frames is increased by an approximate ratio of 62%,44% compared with that in the bare frames, respectively. This indicates a significant decrease in the energy gap when additional stories are added. The S-shaped dampers dissipate 93%, 86%, and 79% of the total energy in cases of 4-, 8-, and 12-story buildings, respectively, indicating their outstanding performance in resisting earthquakes. However, this performance decreases by 8% and 17% as the number of stories increases.

References

Akbar, M., Huali, P., Adedamola, A.-A., Guoqiang, O., Amin, A., 2021. The seismic analysis and performance of steel frame with additional low-yield-point steel dampers. Journal of Vibroengineering 23(3), 647–674. https://doi.org/10.21595/jve.2020.21531

American Institute of Steel Construction, 2016. ANSI/AISC 360-10, Specification for structural steel buildings. AISC.

American Society of Civil Engineers, 2017. Minimum design loads for buildings and other structures (ASCE/SEI 7-10). Reston, VA: American Society of Civil Engineers.

Bruschi, E., Quaglini, V., 2022. Assessment of a novel hysteretic friction damper for the seismic retrofit of reinforced concrete frame structures, in: Structures. Elsevier, pp. 793–811. https://doi.org/10.1016/j.istruc.2022.10.113

Cheraghi, A., Zahrai, S.M., 2019. Cyclic testing of multilevel pipe in pipe damper. Journal of Earthquake Engineering 23(10), 1695–1718. https://doi.org/10.1080/13632469.2017.1387191

Cheraghi, K., TahamouliRoudsari, M., Kiasat, S., 2023. Numerical and analytical investigation of U-shape dampers and its effect on steel frames, in: Structures. Elsevier, pp. 498–509. https://doi.org/10.1016/j.istruc.2023.06.037

CSI, 2021. Components and Elements Manual for PERFORM-3D version.8.

Curadelli, O., Amani, M., 2014. Integrated structure-passive control design of linear structures under seismic excitations. Eng Struct 81, 256–264. https://doi.org/10.1016/j.engstruct.2014.10.002

De Domenico, D., Ricciardi, G., Takewaki, I., 2019. Design strategies of viscous dampers for seismic protection of building structures: a review. Soil dynamics and earthquake engineering 118, 144–165. https://doi.org/10.1016/j.soildyn.2018.12.024

De'nan, F., Hashim, N.S., Abd Wahab, N.A., 2025. Optimizing Structural Connections: Finite Element Analysis of Extended End Plates and Bolt Dynamics. Electronic Journal of Structural Engineering 25(2), 1–8. https://doi.org/10.56748/ejse.24665

Ebadi Jamkhaneh, M., Ebrahimi, A.H., Shokri Amiri, M., 2019. Experimental and numerical investigation of steel moment resisting frame with U-shaped metallic yielding damper. International Journal of Steel Structures 19, 806–818. https://doi.org/10.1007/s13296-018-0166-z

Elhout, E., 2022. Location of semi-rigid connections effect on the seismic performance of steel frame structures. Electronic Journal of Structural Engineering 22(3), 1–10. https://doi.org/10.56748/ejse.223113

Fang, C., Qiu, C., Wang, W., Alam, M.S., 2023. Self-centering structures against earthquakes: a critical review. Journal of Earthquake Engineering 27(15), 4354–4389. https://doi.org/10.1080/13632469.2023.2166163

Federal Emergency Management Agency, 2007. Interim testing protocols for determining the seismic performance characteristics of structural and nonstructural components (FEMA 461). Washington, DC: U.S. Department of Homeland Security.

Foyouzati, A., 2024. Analytical study on seismic strengthening of reinforced concrete frame equipped with steel damping system with shear mechanism fuse. Asian Journal of Civil Engineering 25(1), 1115–1127. https://doi.org/10.1007/s42107-023-00820-0

Fujii, K., 2024. Critical pseudo-double impulse analysis evaluating seismic energy input to reinforced concrete buildings with steel damper columns. Front Built Environ 10, 1369589. DOI: 10.3389/fbuil.2024.1369589

Gagnon, L., Morandini, M., Ghiringhelli, G.L., 2020. A review of friction damping modeling and testing. Archive of Applied Mechanics 90, 107–126. https://doi.org/10.1007/s00419-019-01600-6

Ghadami, A., Ghamari, A., Jaya, R.P., 2024. Improving the behavior of the CBF system using an innovative box section damper: Experimental and numerical study, in: Structures. Elsevier, p. 106210. https://doi.org/10.1016/j.istruc.2024.106210

Ghandil, M., Riahi, H.T., Behnamfar, F., 2022. Introduction of a new metallic-yielding pistonic damper for seismic control of structures. J Constr Steel Res 194, 107299. https://doi.org/10.1016/j.jcsr.2022.107299

Gholami, M., Deylami, A., Tehranizadeh, M., 2013. Seismic performance of flange plate connections between steel beams and box columns. J Constr Steel Res 84, 36–48. https://doi.org/10.1016/j.jcsr.2012.11.011

Guo, K., Pianese, G., Pan, P., Milani, G., 2025a. Influence of Geometrical Features on the Cyclic Behavior of S-Shaped Steel Dampers Used in Sustainable Seismic Isolation: Experimental Insight with Numerical Validation. Sustainability 17(2), 660. https://doi.org/10.3390/su17020660

Guo, K., Pianese, G., Valente, M., Pan, P., Milani, G., 2025b. Experimental and numerical investigation of elastomeric seismic isolators coupled with S-

shaped steel dampers, in: Structures. Elsevier, p. 109472. https://doi.org/10.1016/j.istruc.2025.109472
Haider, S.M.B., Lee, D., 2021. A review on BRB and SC-BRB members in building structures. Struct. Eng. Mech 80(5), 609. https://doi.org/10.12989/sem.2021.80.5.609
Hibbitt, Karlsson, Sorensen, 2022. Abaqus/CAE User's Manual. Hibbitt, Karlsson & Sorensen, Incorporated.
Hsu, H.-L., Halim, H., 2018. Brace performance with steel curved dampers and amplified deformation mechanisms. Eng Struct 175, 628–644. https://doi.org/10.1016/j.engstruct.2018.08.052
Jaisee, S., Yue, F., Ooi, Y.H., 2021. A state-of-the-art review on passive friction dampers and their applications. Eng Struct 235, 112022. https://doi.org/10.1016/j.engstruct.2021.112022
Javanmardi, A., Ibrahim, Z., Ghaedi, K., Ghadim, H.B., Hanif, M.U., 2019. State-of-the-art review of metallic dampers: testing, development and implementation. Archives of Computational Methods in Engineering 1–24. https://doi.org/10.1007/s11831-019-09329-9
Jeong, S.-H., Ghamari, A., Ince, G., 2024. A comparative experimental and numerical study on the shear and flexural mechanism of an innovative butterfly-damper. J Constr Steel Res 222, 108979. https://doi.org/10.1016/j.jcsr.2024.108979
Ke, K., Yam, M.C.H., Zhang, P., Shi, Y., Li, Y., Liu, S., 2023. Self-centring damper with multi-energy-dissipation mechanisms: Insights and structural seismic demand perspective. J Constr Steel Res 204, 107837. https://doi.org/10.1016/j.jcsr.2023.107837
Khoshkalam, M., Mortezagholi, M.H., Zahrai, S.M., 2022. Proposed modification for ADAS damper to eliminate axial force and improve seismic performance. Journal of earthquake engineering 26(10), 5130–5152. https://doi.org/10.1080/13632469.2020.1859419
Mohammadi, R.K., Nasri, A., Ghaffary, A., 2017. TADAS dampers in very large deformations. International Journal of Steel Structures 17, 515–524. https://doi.org/10.1007/s13296-017-6011-y
Pan, Y., Gao, H., Zeng, H., Li, Y., 2024. Study on energy dissipation performance of low-yield-point steel shear panel dampers. J Constr Steel Res 213, 108351. https://doi.org/10.1016/j.jcsr.2023.108351
Rakan-Nasrabadi, T., Pourmahdi-Tazeabadi, S., karimi-gabalou, S., haghollahi, A., 2025. Investigating lateral behavior of the hybrid system of flat steel shear walls and cold-formed S-shaped steel plate dampers under cyclic loading. Iranian Journal of Science and Technology, Transactions of Civil Engineering 49, 3927–3951. https://doi.org/10.1007/s40996-024-01657-6
Saaed, T.E., Nikolakopoulos, G., Jonasson, J.-E., Hedlund, H., 2015. A state-of-the-art review of structural control systems. Journal of Vibration and Control 21(5), 919–937. https://doi.org/10.1177/1077546313478294
Sahoo, D.R., Singhal, T., Taraithia, S.S., Saini, A., 2015. Cyclic behavior of shear-and-flexural yielding metallic dampers. J Constr Steel Res 114, 247–257. https://doi.org/10.1016/j.jcsr.2015.08.006
Shen, H., Zhang, R., Weng, D., Gao, C., Luo, H., Pan, C., 2017. Simple design method of structure with metallic yielding dampers based on elastic–plastic response reduction curve. Eng Struct 150, 98–114. https://doi.org/10.1016/j.engstruct.2017.07.047
Shu, Z., You, R., Zhou, Y., 2022. Viscoelastic materials for structural dampers: A review. Constr Build Mater 342, 127955. https://doi.org/10.1016/j.conbuildmat.2022.127955
Wang, Y., Guo, C., You, P., Wu, H., Wang, Z., Li, Y., 2024. Seismic performance of prefabricated composite shear wall with end steel plate connection by nonlinear finite element analysis. Electronic Journal of Structural Engineering 24(2). https://doi.org/10.56748/ejse.24557
Zhai, Z., Guo, W., Yu, Z., He, C., Zeng, Z., 2020. Experimental and numerical study of S-shaped steel plate damper for seismic resilient application. Eng Struct 221, 111006. https://doi.org/10.1016/j.engstruct.2020.111006
Zhai, Z., Li, S., Liu, Y., Ma, Y., Zou, S., Zhou, F., 2022. Seismic retrofitting of SMRFs using varied yielding cross-section damper: A companion paper. J Constr Steel Res 194, 107290. https://doi.org/10.1016/j.jcsr.2022.107290
Zhang, C., Zhou, Y., Weng, D.G., Lu, D.H., Wu, C.X., 2015. A methodology for design of metallic dampers in retrofit of earthquake-damaged frame. Struct. Eng. Mech 56(4), 569–588. http://dx.doi.org/10.12989/sem.2015.56.4.56
Zhang, H., Li, A., Su, Y., Xu, G., Sha, B., 2024. Viscoelastic dampers for civil engineering structures: A systematic review of constructions, materials, and applications. Journal of Building Engineering 96, 110597. https://doi.org/10.1016/j.jobe.2024.110597
Zhang, R., Wang, C., Pan, C., Shen, H., Ge, Q., Zhang, L., 2018. Simplified design of elastoplastic structures with metallic yielding dampers based on the concept of uniform damping ratio. Eng Struct 176, 734–745. https://doi.org/10.1016/j.engstruct.2018.09.009
Zhao, B., Lu, B., Zeng, X., Gu, Q., 2021. Experimental and numerical study of hysteretic performance of new brace type damper. J Constr Steel Res 183, 106717. https://doi.org/10.1016/j.jcsr.2021.106717
Zhao, J.-Z., Tao, M.-X., Wu, Z.-H., Zhuang, L.-D., 2022. Experimental and numerical study on bent shear panel damper made of BLY160 steel. Eng Struct 260, 114229. https://doi.org/10.1016/j.engstruct.2022.114229
Zhu, B., Wang, T., Zhang, L., 2018. Quasi-static test of assembled steel shear panel dampers with optimized shapes. Eng Struct 172, 346–357. https://doi.org/10.1016/j.engstruct.2018.06.004
Zhu, Y., Wang, W., Lu, Y., Yao, Z., 2023. Finite element modeling and design recommendations for low-yield-point steel shear panel dampers. Journal of Building Engineering 72, 106634. https://doi.org/10.1016/j.jobe.2023.106634

Disclaimer